Experimental Mechanics (2018) 58:1207–1219
https://doi.org/10.1007/s11340-018-0402-7

A New Multiaxial Specimen for Determining the Dynamic Properties of Adhesive Joints

A. Janin[1,2] · A. Constantinescu[1] · D. Weisz-Patrault[1] · R. Neviere[2] · M. Stackler[2] · W. Albouy[2]

Received: 10 November 2017 / Accepted: 14 May 2018 / Published online: 31 May 2018

Abstract

Adhesive joints are increasingly employed for bonding critical parts of industrial structures. Therefore, adhesive joints become a key element in design, and their mechanical characterization is of the utmost importance. Significant advancement has been realized for their characterization under quasi-static loadings; however characterization techniques are rather limited for dynamic loadings. Indeed, due to the complex paths of waves through structures, existing dynamic characterization techniques will not characterize only the adhesive joint, but instead will characterize the complete assembly containing the joint and the adherents. Moreover, multiaxiality control of the loading on the adhesive joint is difficult to achieve. This paper proposes an innovative experimental technique for the characterization of adhesive joints under dynamic multiaxial loadings. The experimental method relies on three main components: i) a conventional split Hopkinson pressure bar (SHPB) apparatus, ii) a novel specimen, denoted as *DODECA*, which enables testing of three distinct multiaxial loadings using the same method and iii) local strain and stress measurements performed by digital image correlation (DIC). The paper describes all steps of the experimental procedure, including the underlying preparation of the specimen and the measuring methods. The stress and strain in the adhesive joint are estimated directly from the experimental data both during loading and at the failure point. Finally, the dynamic material behavior of the adhesive joint is identified from the data.

Keywords Adhesive joints · *DODECA* specimen · Dynamic loading · Digital image correlation

Introduction

In recent decades, under the constraints of energy efficiency and lightening of structures, especially for aeronautical applications, the assembly of composite elements using adhesive joints emerged as an interesting alternative to conventional methods such as riveting or screwing. However, the mechanical behavior of adhesive joints is neither sufficiently understood nor characterized to obtain certifications for critical structural assemblies. Therefore, elucidating the mechanical behavior of adhesive joints is an essential requirement in order to model assemblies of industrial parts. Moreover, bonded joints are subject to wide ranges of loading conditions: quasi-static and dynamic multiaxial loadings, thermomechanical fatigue or aging.

This work presents an innovative experimental characterization of adhesive joints under dynamic multiaxial loadings. In the past, significant efforts have been made under quasi-static loadings as reported, for example, in [1, 2].

However, the existing studies under dynamic loading conditions use the single-lap joint specimen [3] or the double-lap joint specimen [4, 5], which only investigate the shear behavior of adhesive joints. As a consequence, the extension of the results for more complex multiaxial loading conditions is still rather limited. The extension to multiaxial loadings is critical, as it is generally known that the mechanical behavior of polymeric materials is stress-dependent. For example, the variation in yield strength with multiaxiality is described in [6]. Further difficulty arises because the dynamic tests are usually performed on the split Hopkinson pressure bar (SHPB) apparatus that provides only global mechanical measurements: the displacements and resultant forces at both ends of the

✉ A. Constantinescu
andrei.constantinescu@polytechnique.edu

A. Janin
anthony.janin@polytechnique.edu

[1] LMS, École Polytechnique, Université Paris-Saclay, Palaiseau, France

[2] Safran Composites, Itteville, France

specimen. This characterizes not only the adhesive joint but also the complete assembly including the structure of the specimen and the boundary contact conditions (see [3–5] for further discussions on these questions). As a consequence, an additional local measurement of the involved mechanical fields during the dynamic testing is of great interest.

The aim of this work is to characterize the dynamic behavior of adhesive joints using a SHPB system and to overcome the two abovementioned difficulties :

1) multiaxial loading conditions are introduced by proposing a novel experimental setup that easily handles different normal to shear stress ratios on the joint;
2) a local measurement system with high spatial and temporal resolutions is added to the data-deficient classical SHPB data acquisition to provide relevant information about the adhesive joint.

One option to overcome the first difficulty, i.e., to create multiaxial loading conditions, is to use torsional [7] or tensile [8] Hopkinson bar systems. However, each experimental apparatus provides only one loading direction in the multiaxial stress space and the exploration of several stress directions remains difficult. Another option is to perform standard dynamic compression tests by using conventional SHPB systems and to create multiaxial stress states on the adhesive joint through a structural effect caused by the specimen geometry. Different specimen geometries have been proposed for homogeneous materials (i.e., without an adhesive joint) and optimized for a well-defined stress state. For instance, the *compact compression specimen* (CCS) [9] was designed to study dynamic fracture initiation and propagation under a concomitant large traction and low shear stress at the crack tip. The main advantage of this specimen geometry is that is necessitate only a conventional compression Hopkinson bar system although significant traction is produced. Likewise, the *shear compression specimen* (SCS) [10] was designed for the characterization of thick polymer films ($\approx 2\ mm$) under a biaxial stress state of compression and shear. Similarly, the characterization of metals under a biaxial stress state is carried out using a *shear tension specimen* (STS) [11]. Equally important, the *double edge notched compression specimen* (DENCS) [12] has been used for measuring compressive fracture toughness in dynamic tests.

For characterizing the material toughness under a multiaxial dynamic loading condition, it is the *Brazilian disk* (BD) specimen has become popular [13, 14]. Several authors proposed an interesting modification in order to adapt the original BD specimen for bonded assemblies under quasi-static loadings. One of the specimen design is the *sandwich Brazilian disk* (SBD), as discussed in [15, 16]. This specimen offers an infinite number of possible stress states when the impact angle in the SHPB system is varied. The present contribution is inspired by the SBD specimen and proposes to change the SBD disk into a dodecagon. This change was introduced to obtain a plane-to-plane contact between the bars and the specimen, simplifying experimental and numerical procedures. The suggested specimen is therefore a sandwich dodecahedron, denoted as the *DODECA* specimen. As constructed, the specimen geometry enables three different impact angles leading to three different stress states in the adhesive joint. This geometry has already been briefly discussed in [17]. The specific shape of the present contribution introduces a new version of the *DODECA* specimen; this new version avoids edge effects and regularizes the stresses at both ends of the adhesive joint.

Several local measurement systems can be used to overcome the second difficulty, i.e., the data deficiency of the classical SHPB data acquisition; a local measurement system with high spatial and temporal resolutions is added to provide relevant information about the adhesive joint. In dynamic testing, several options are available: Moiré interferometry [18], crack growth photography [19] and digital image correlation (DIC). For practical reasons, we use a DIC method, as it has already proven its potential both in quasi-static measurements [20, 21] and dynamic measurements [8, 22–24] in recent years. The transition from quasi-static to dynamic conditions has been possible through the technological advances in high-speed acquisition from imaging systems. In this work, a high-speed camera is used to provide a series of images, enabling the measurement of local displacements by DIC. Due to technological limitations of the image acquisition system, a compromise has to be found between acquisition frequency and spatial resolution. To obtain optimal measurements, particular attention is given to speckle pattern techniques [25]. As a consequence of the different choices in methodology, we were able to achieve micrometer resolution in the present work.

The paper is organized as follows. The SHPB system is briefly described in Section "Dynamic Testing". Then, the innovative *DODECA* specimen is presented in Section "DODECA Specimen". The local measurement setup in the adhesive joint is detailed in Section "Digital Image Correlation". Finally, the results are presented and discussed in Section "Results and Discussion".

Dynamic Testing

The dynamic testing is performed using a SHPB apparatus and a traditional data acquisition and analysis method. For a detailed review of this method, we suggest the classical literature on the subject, for example [26–29]. The conventional configuration of the Hopkinson bar system is

made of two 40 mm-diameter high-strength aluminum bars. The 86 or 120 cm long striker bars are made of the same aluminum material and have the same diameter as both the input and the output bars. The output bar is 2 m long, and the input bar is 3 m long in order to allow longer acquisition of the loading signals. The *DODECA* specimen is placed between the input and the output bars, as shown in Fig. 1. The displacements and resultant forces at the ends of the specimen, more precisely at the bar-specimen interfaces, are determined from strain measurements recorded at the gauge stations placed at different positions on the bars.The gauge stations provide a 1 MHz acquisition frequency. The post-processing of the strain signals was carried out with the DAVID software [30]. It includes several functions that ensure noise filtering, checking the balances of forces and energy, providing elastic simulation for an accurate transport of elastic waves to the interfaces, wave dispersion and local punching correction [31]. This Hopkinson bar configuration was used for impact velocities between 5 and 15 m/s measured on the striker with a laser beam system. Silicon grease is applied between the specimen and the bars in order to avoid shear stress at the specimen-bar interface contact. In addition, a 50 μm-thick pulse shaper is fixed on the input bar. This technique produces a more constant strain rate by limiting high strain rates at the beginning of the test. Consequently, this improves test repeatability.

DODECA Specimen

Geometry

This section presents the novel *DODECA* specimen. It is a sandwich-dodecahedron, i.e., a dodecahedron split in two by the adhesive joint, with an outer circumscribed diameter of 40 mm. The specimen is machined out of a 10 mm-thick aluminum plate and the two parts are bonded by a 300 μm-thick adhesive joint. For the test, adherent parts have to be very rigid compared to the adhesive joint, and the adhesive joint has to be very thin compared to adherent size. The main features are similar with the initial design already discussed in [17]. The previous design presented edge effects in the adhesive joint, as already reported in the case of quasi-static characterization of adhesive joints [1, 2]. The present shape introduced sharp beaks near both edges of the joint as shown in Fig. 2. This modification permits to regularize the stress field in these zones and introduces a stress relaxation at the edges. The angles of the outer edges of the dodecahedron define implicitly three impact angles, labeled as: 15° 45° and 75°. This geometry proved to be well suited for the 45° and 75° impact conditions. More specifically, the 15° impact condition needs a further adjustment. The machined beaks at the edges of the joint reduce the contact surface between the specimen and the Hopkinson bars. As a consequence, the contact surfaces are not aligned any more with the center of mass of the specimen. Therefore, the misalignment introduces a spurious torque as shown on the left part of Fig. 3, which induces a rotation of the specimen from the very beginning of the impact loading. The reduction of the contact surfaces, as shown on the right part of Fig. 3, restores the alignment of resultant force with the mass center of the specimen and removes the torque.

Furthermore, as shown in Section "Numerical Simulation", the multiaxial stress state for the 75° loading condition is highly compressive when compared with the shear component. In this case, it can occur that failure of the joint cannot be reached, due to the high compressive stress. Therefore, if failure of the joint is studied, dedicated specimens can be manufactured, were the adhesive joint is bonded to the parts of the dodecahedron only in the middle on a small section of approximatively 12 mm.

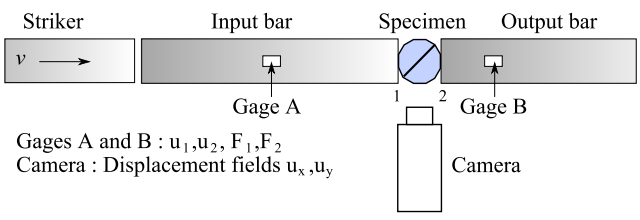

Fig. 1 Experimental setup scheme of the SHPB apparatus and the local optical measurement system

Fabrication

As specified above, the *DODECA* specimen is finally manufactured by bonding the two aluminum parts to the adhesive joint. The difficulty of this operation is to ensure a constant thickness of the joint. To control the thickness of the joint, a special assembly device has been devised and is displayed in Fig. 4. This assembly device is an improved version of the initial bonding device presented in [17] which

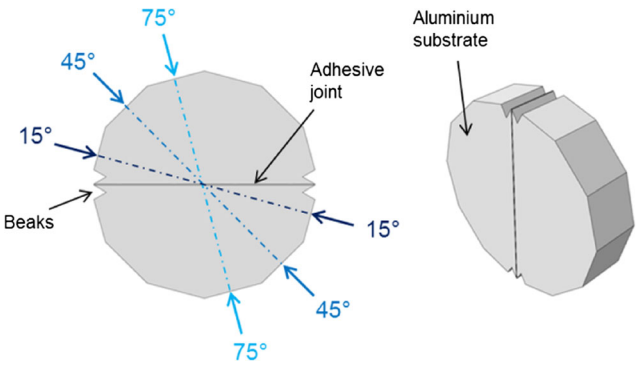

Fig. 2 Schematic view of the *DODECA* specimen

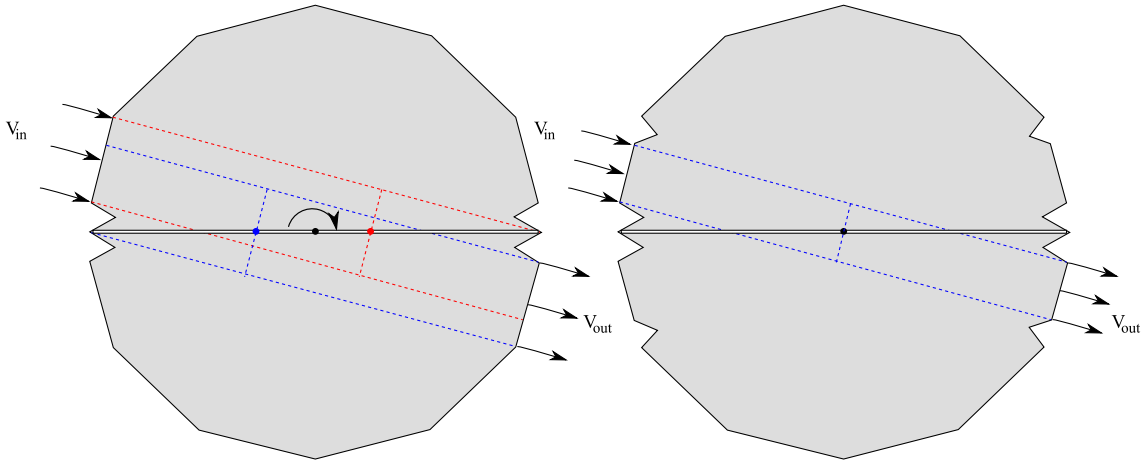

Fig. 3 Geometrical adjustments to avoid rotation for the 15° loading condition

improved the accuracy and homogeneity of the adhesive thickness all along the specimens. Five assemblies allow the concomitant preparation of five samples. Two lateral screws apply pressure on two faces of the dodecahedron in order to keep the adherents in the jig. Two vertical centering screws are used to apply pressure on the specimens in the normal direction of the adhesive joint during the whole curing process. Satisfying the alignment of both adherents is ensured. The joint thickness is controlled by introducing 300 μm-thick shims as shown in Fig. 4. The bonding procedure can be summarized as follows:

1) The release agent is applied with a brush on the shims and inside the jig where there is contact between the jig and the adherent. Subsequently, these components are left for 10 minutes under a hood for drying.
2) The adherents are mounted in the jig and the bottom parts should be 200 μm above the reference flat surface of the jig. If this value is not reached due to machining tolerances, Teflon adhesive tape is applied underneath in order to raise the lower adherent to the nominal value.
3) Lateral screws are tightened in order to avoid slippings during the curing process.
4) The bonding surfaces are still 200 μm above the reference surface. Thus, they are ground until they are flush with the reference level of the jig with a P600 carbide sand paper.
5) The bonding surfaces are first washed with water, then washed three times with isopropanol and finally left to dry for 10 minutes under a hood.
6) The release agent is applied on all the remaining surfaces, i.e., the surfaces that should not be bonded.
7) The adhesive joint is a thin film that is cut into 10 × 39 mm pieces with a sharp knife. The film is then applied to one surface for bonding.
8) The vertical screws are tightened until the shims are blocked.
9) The joint is cured at 150° C for 3 hours, and the excess glue is cut off at the end of the curing process.
10) The lateral faces are polished in order to facilitate the DIC.

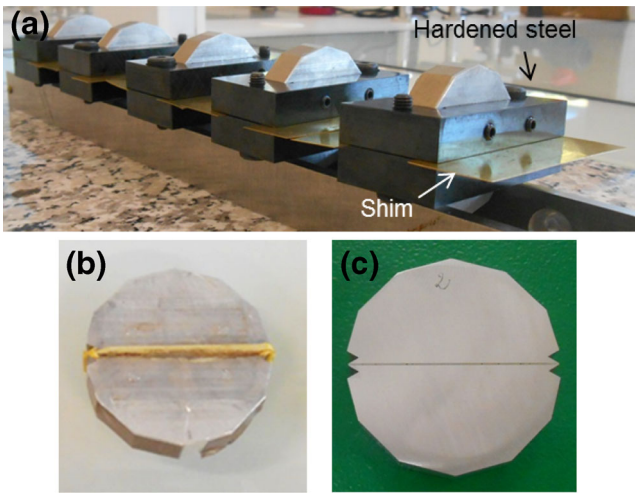

Fig. 4 (**a**) Specimens before curing and bonding devices. (**b**) Specimen just after curing. (**c**) Final specimen ready for testing

The quality of the adhesive bond is estimated by digital microscopy. A typical image is shown in Fig. 5. The obtained samples present few air bubbles (5% of the lateral surface) and the average joint thickness is 300 μm with variations of ±6% along the length of the entire joint.

Numerical Simulation

Numerical simulations were used to design the *DODECA* specimen. More specifically, two-dimensional elastic finite element computations were performed with ABAQUS software [32]. The reduction of the spatial dimension

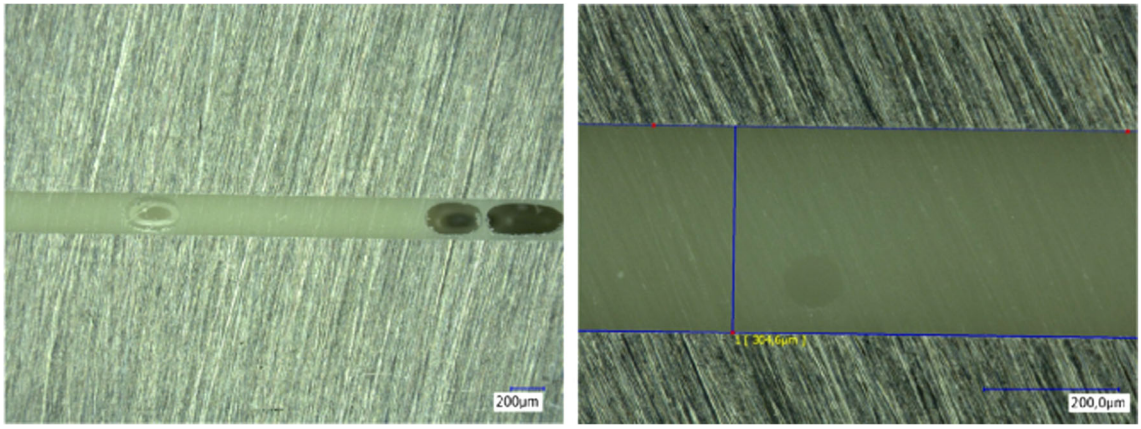

Fig. 5 Digital microscopy of the adhesive joint: view of defects in the adhesive joint and measurement of the adhesive thickness

from 3 to 2 is justified by the computational cost of the problem. The stress distribution along the adhesive joint was evaluated as a function of time for 15°, 45° and 75° loading conditions. Furthermore, a very simplified Hopkinson bar impact was modeled by imposing displacements of 100 μm along the normal direction of the input specimen surface and by blocking displacements at the output specimen surface. The mesh consisted of 80 000 nodes assembled with 4-node reduced integration elements (CPS4R). The material behaviors of both the adhesive joint and the substrate were considered to be elastoplastic. To maintain a high accuracy of the interface and bulk stresses, 10 elements were employed to represent the thickness of the adhesive joint.

In these computations, the aim is not to reproduce a Hopkinson bar experiment accurately but is to determine the stress distribution in the joint with a typical loading condition in terms of amplitude. More representative models [4, 10] could also be used to analyze the stress distribution in this experiment but require a significant calculation time. Results are presented in Figs. 6, 7 and 8. It should be noted that x and y denote the joint length and the joint thickness directions, respectively. All the computed stress distributions are heterogeneous and exhibit a critical stress state at the joint center. The edges of the joint are unloaded. Table 1 summarizes the three stress distributions according to the loading angle of the *DODECA* specimen.

Moreover, as mentioned in Section "Geometry", the proposed specimen shape has beaks at the edges of the joint to avoid stress singularities. The effect of this specific geometrical adjustment is presented in Figs. 9 and 10. Adding beaks does not change the stress distribution but does eliminate edge effects as expected. Indeed, analytical approaches have proven that substrates with beaks (substrate angle $\leq 50°$) reduce stress singularities, as discussed in [33, 34].

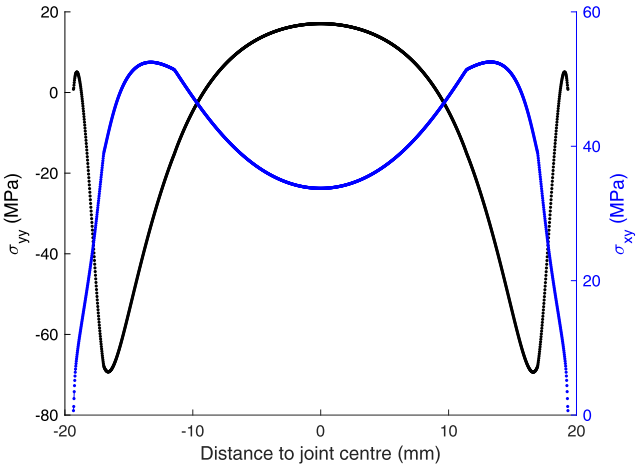

Fig. 6 Numerical simulation: normal stress σ_{yy} (*black line*) and shear stress σ_{xy} (*blue line*) versus distance to the joint center for the 15° loading condition

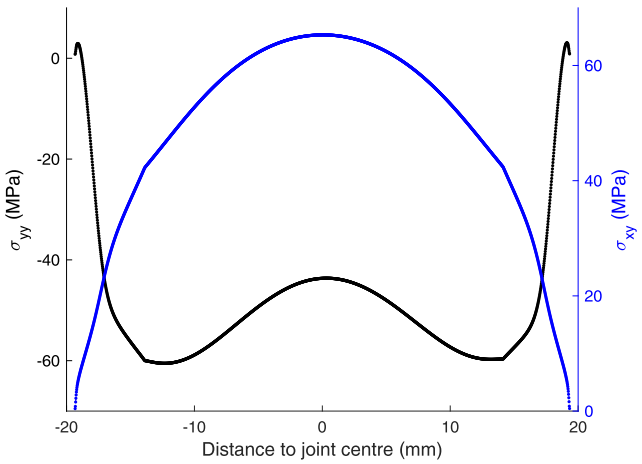

Fig. 7 Numerical simulation: normal stress σ_{yy} (*black line*) and shear stress σ_{xy} (*blue line*) versus distance to the joint center for the 45° loading condition

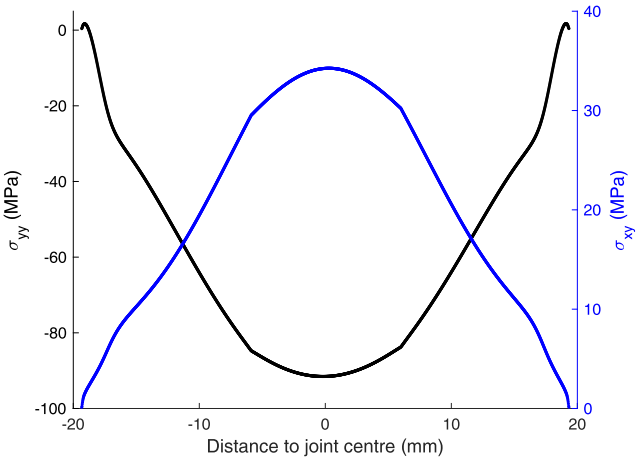

Fig. 8 Numerical simulation: normal stress σ_{yy} (*black line*) and shear stress σ_{xy} (*blue line*) versus distance to the joint center for the 75° loading condition

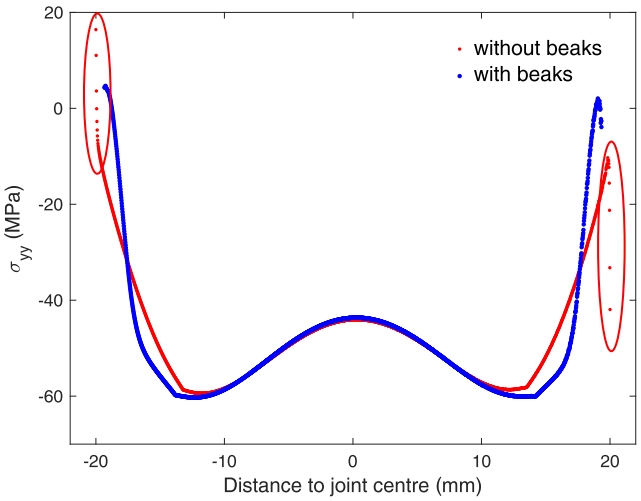

Fig. 9 Numerical simulation: normal stress σ_{yy} as a function of distance to joint center, with and without beaks. The encircled points represent the values eliminated by the presence of the beaks

Digital Image Correlation

A local displacement and strain measurement method is added to the data acquisition of the experiment by adding a camera coupled with a digital image correlation (DIC) program. Since the duration of the test is a few hundreds μs, a high-speed imaging acquisition system is needed. A fast estimation showed that the temporal resolution should be at least 70 000 frames per second (fps). Therefore, in dynamics, there is a compromise to be made between the spatial resolution and the acquisition frequency of the pictures. In standard quasi-static studies, one can provide high-spatial-resolution images, for instance: 2048×2048 pixels, to apply DIC. In dynamics, this resolution cannot be reached because of the very high temporal resolution needed. To improve the performance of the system, i.e., to obtain high-quality DIC measurements with a low spatial resolution, the contrast of images must be optimal. Thus, particular attention has been given to the lighting techniques and the applied speckle pattern. A very powerful lighting is required in the area of interest due to the low exposure time. Here, a halogen flashlight, triggered with the input strain gauge, has been used to overcome this issue. Furthermore, a speckle pattern is applied with an airbrush on the specimen face by using high-strain-rate-resistant paint. The best results were obtained by first applying a homogeneous white coat and then applying a black speckle pattern with a typical size of 150 μm. The speckle size was measured with a digital microscope.

Technical information is summarized in Table 2. Images are processed with the Vic2D software using 9 × 9 pixel subset for measuring the displacements. This size was chosen to obtain a reasonable displacement resolution in the substrate areas. Subsets that are too large propagate high displacements from the adhesive joint to the substrates. For measuring strains, larger subsets (a 21 × 21 pixel subset) are used because of the higher noise present in the strain field. The imaging area is presented in Fig. 11. For 15° and 45° loading conditions, the imaging area is initially shifted from the joint plane of 10 pixels in order to take

Table 1 Summary of available stress distributions with the *DODECA* specimen

Loading angle (°)	Shear	Compression	Tension
15	High	None	Medium
45	High	Medium	None
75	Medium	High	None

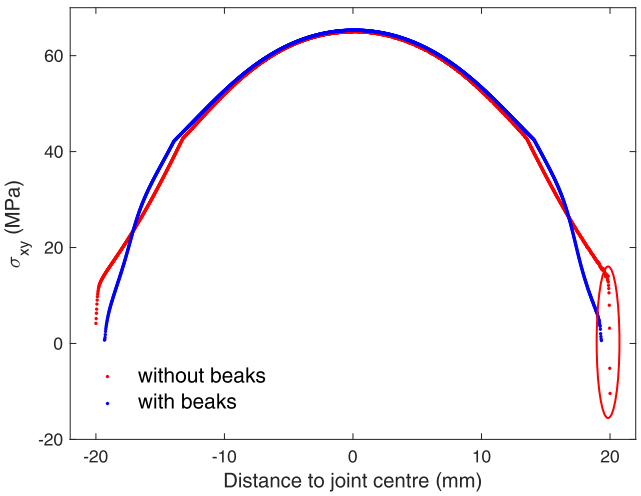

Fig. 10 Numerical simulation: shear stress σ_{xy} as a function of distance to joint center, with and without beaks. The encircled points represent the values eliminated by the presence of the beaks

Table 2 High-speed imaging parameters

Camera	Phantom v7.3
Lighting	Visatec SOLO 1600 B (halogen flashlight, 150 W)
Lens	Nikon 105 mm f 2.8 1:1
Exposure time	1 μm
Time between 2 images	13-14 μs
Resolution 15° and 45°	416×80 pixels (1 px$\simeq$ 52 μm)
Resolution 75°	196×144 pixels (1 px$\simeq$ 55 μm)
Software DIC	Vic2D
Subset displacements	9 pixels (step : 1 px)
Subset strains	21 pixels (step : 1 px)

into account the rigid body motion of the specimen during the SHPB test. For the 75° loading condition, the rigid body motion is more significant, and the imaging zone is changed to focus on only the central zone of the specimen. In addition, the imaging area is initially shifted from the joint plane by 30 pixels. A picture of the experimental setup is shown in Fig. 12 and includes the camera, painted specimen, Hopkinson bar system and plexiglass protection. An additional flexible lighting system is required to calibrate the imaging area before the test. Considering that the pixel size is 52 μm or 55 μm and that the joint thickness is 300 μm, it follows that this experimental setup does not enable us to directly measure the local displacements in the adhesive joint. However, displacement fields in the adherents, as well as the gradients, near the adhesive joint are measured accurately. Therefore, only a global mean through-thickness strain, i.e., homogeneous along the joint thickness, can be estimated on this basis.

Results and Discussion

This paper focuses on developing a methodology to characterize adhesive joints under dynamic and multiaxial loading conditions. Thus, the following experimental results demonstrate the potential offered by the proposed methodology and do not aim to contribute to any material data base. Due to confidentiality constraints, most scales are normalized by arbitrary values in the following discussion.

Global Measurements

This section presents the standard results obtained with the Hopkinson bar system. Several tests have been performed for each loading condition. The resultant (normalized) force obtained at the specimen/output bar interface is presented as a function of time for the three loading conditions in Figs. 13, 14 and 15. The parameters used for the different tests and loading conditions are summarized in Tables 3, 4 and 5. The obtained signals are very similar for each loading condition. The differences are mainly due to the variability in the striker velocities. The duration of the test decreases with increasing striker velocity. In the experiment, the duration of the test is limited by the failure of the adhesive joint. Otherwise, in standard tests, the duration is completely determined by the length of the striker. Most presented tests have been performed with an 86 cm long striker which corresponds to a 350 μs test duration. In Figs. 13, 14 and 15, the failure of the joint is reached before the final duration of the test, as computed from the striker length. In this case, the force drop corresponds to the failure of the adhesive joint. In addition, the discrepancies observed

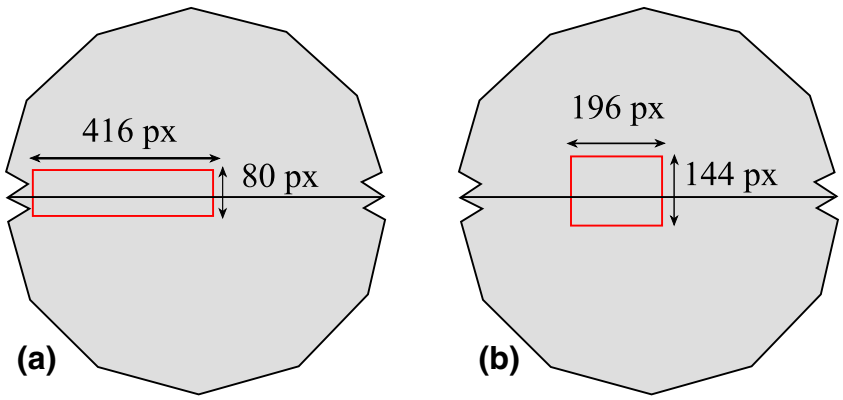

Fig. 11 **a** Imaging area for the 15° and 45° loading conditions. **b** Imaging area for the 75° loading condition

Fig. 12 Photograph of the experimental set-up

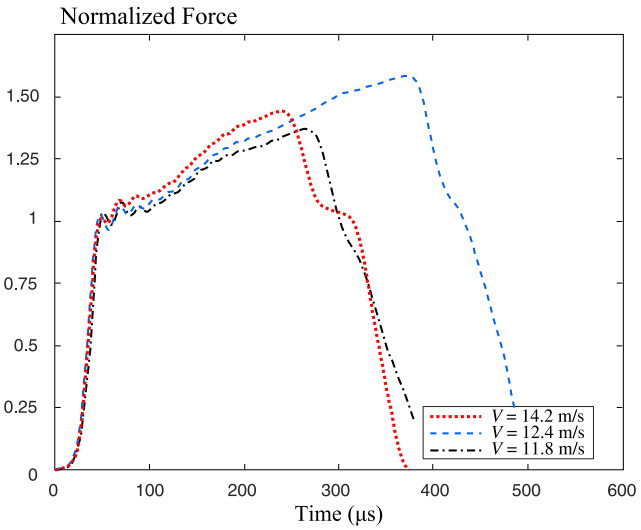

Fig. 14 Normalized force as a function of time for the 75° loading condition

in Figs. 13, 14 and 15 can be explained, to a lesser extent, by the contact conditions, specimen/bar alignment, specimen geometry (e.g, joint thickness) and material variability. Global strain rates between 700 and 1500 s^{-1}, depending on the striker velocity, are evaluated from the Hopkinson tests.

The strength of the assembly, expressed as the maximal force reached during the experiment, is highly repeatable. Its standard deviation was evaluated to 2.6 % of the average normalized strength for the 45° loading condition. The two other loading angles exhibit similar standard deviations of the strength of the assembly. The 15° loading leads to the lowest strength because of the mixed traction/shear stress state. The 75° loading leads to the highest strength as a consequence of the high compressive stress component present during this experiment. Furthermore, let us remember that this global measurement characterizes the complete assembly, adherents and adhesive joint together, and that an additional local measurement is required to characterize the adhesive joint.

Local Measurements

The striker velocities have been chosen so that 15 to 20 images can be recorded during the test before joint failure. The image acquisition is triggered by signal detection at the input strain gauge. Horizontal displacements denoted by u are presented in Fig. 16 for the 45° loading condition

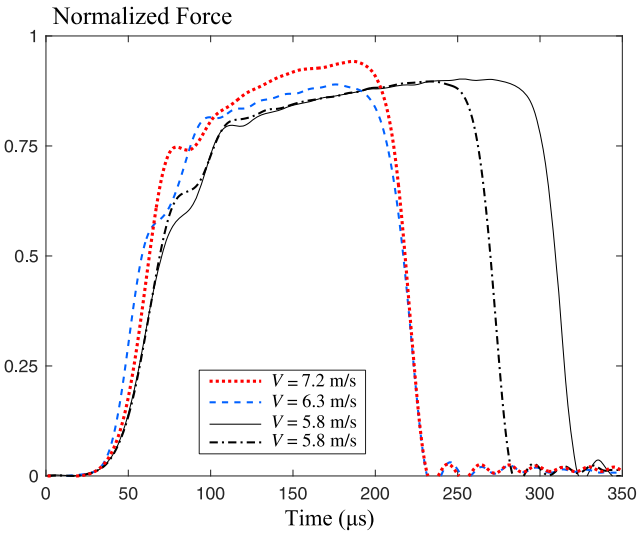

Fig. 13 Normalized force as a function of time for the 45° loading condition

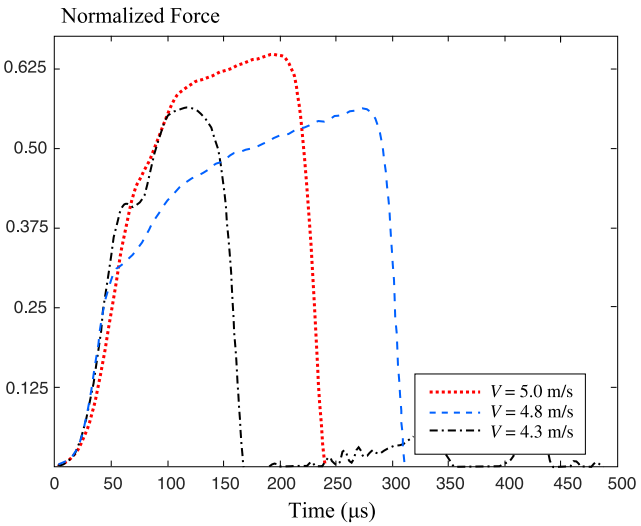

Fig. 15 Normalized force as a function of time for the 15° loading condition

Table 3 Summary of four tests for the 45° loading condition

Striker length (cm)	Striker velocity (m/s)	Normalized strength
86	7.2	0.94
86	6.3	0.89
86	5.8	0.90
86	5.8	0.895

and $V = 5.8$ m/s at different time instants: 1 μs, 14 μs, 41 μs and 180 μs. White squares are used as virtual gauges and indicate the center of the specimen just above and underneath the joint. The displacement amplitude increases with time. The displacement jump between the two adherents is associated with the global shear strain in the adhesive joint. Moreover, the displacements are qualitatively consistent with the numerical simulations presented in Fig. 7, where the shear stress is greatest at the center and decreases near the specimen edges. This is illustrated in Fig. 17 more precisely. In the last displacement field at 180 μs, one can notice zones where DIC could not be applied, i.e., the gray zones along the joint, because the local deformations were large enough to chip the paint off.

Vertical displacements denoted by v are presented in Fig. 16 for the 45° loading condition and $V = 5.8$ m/s at 180 μs. This displacement field is more difficult to interpret because there is no significant displacement jump (extremum lies between 353 and 320 μm). However, the accuracy is sufficient to qualitatively observe the compression evolution along the joint length. At the center (white squares), it is characterized by the difference between blue and green zones, resulting in a low compression. The compression increases toward the edge until it reaches a maximum characterized by the difference between blue/green and red zones and decreases at the very edge. This qualitative evolution is consistent with the numerical simulations presented in Fig. 7.

Consider (x, y, z) as Cartesian coordinates corresponding to the joint length, the joint thickness and the joint depth directions, respectively. Strains are computed from the symmetric part of the displacement gradient. The strain fields could be obtained directly from DIC by considering the gradient of the displacements. However, measurement

Table 4 Summary of three tests for the 75° loading condition

Striker length (cm)	Striker velocity (m/s)	Normalized strength
120	12.4	1.6
120	11.9	1.37
86	14.2	1.44

Table 5 Summary of three tests for the 15° loading condition

Striker length (cm)	Striker velocity (m/s)	Normalized strength
86	5.0	0.65
86	4.3	0.56
86	4.8	0.56

noise is amplified by this numerical procedure. In this contribution, a simplified analysis enables us to overcome this difficulty. Since only surface measurements are available, it is assumed that displacements are homogeneous along the z-direction. Thus, displacements along x and y denoted by u^* and v^* depend only on x and y in the specimen, and the displacements along z are set to zero. The superscript * indicates that the quantity is related to the adherent; otherwise, the quantity is considered for the adhesive joint. Moreover, as already mentioned, the spatial resolution is not sufficient to directly measure displacements in the joint. Thus, strains in the joint are assumed to be independent in the y-direction and are only related to the following displacement variations (where h denotes the joint thickness):

$$\begin{cases} \Delta u(x) = u^*(x, h/2) - u^*(x, -h/2) \\ \Delta v(x) = v^*(x, h/2) - v^*(x, -h/2) \end{cases} \tag{1}$$

Then, displacements u and v in the joint are assumed to be linear and a function of y:

$$u(x) = \frac{\Delta u(x)}{h} y + f_u(x) \text{ and } v(x) = \frac{\Delta v(x)}{h} y + f_v(x) \tag{2}$$

Functions $f_u(x)$ and $f_v(x)$ may be evaluated in Fig. 16. Since the strains in this study are evaluated at the joint center (i.e., using the displacements from the virtual gauges in Fig. 16), $f_u(x)$ and $f_v(x)$ are neglected. Moreover, variations in $h\Delta v(x)$ along the x-directions are assumed to be negligible compared to the variations in $\Delta u(x)$, more precisely:

$$\Delta u(x) \gg h \frac{\partial \Delta v(x)}{\partial x} \tag{3}$$

Thus, by combining (equations (1)) and (2), the strain tensor that should be identified along the joint length reads:

$$\varepsilon_{xy}(x) = \frac{\Delta u(x)}{2h} \text{ and } \varepsilon_{yy}(x) = \frac{\Delta v(x)}{h} \tag{4}$$

Normalized shear and normal strains are presented as a function of time at the joint center in Figs. 18 and 19 for the 15°, 45° and 75° loading conditions and for $V = 5.0$, $V = 5.8$ and $V = 14.2$ m/s, respectively. These time evolutions are consistent with the previous numerical analysis and the three expected stress states described in Table 1. The virtual gauges (15-pixel white squares) can

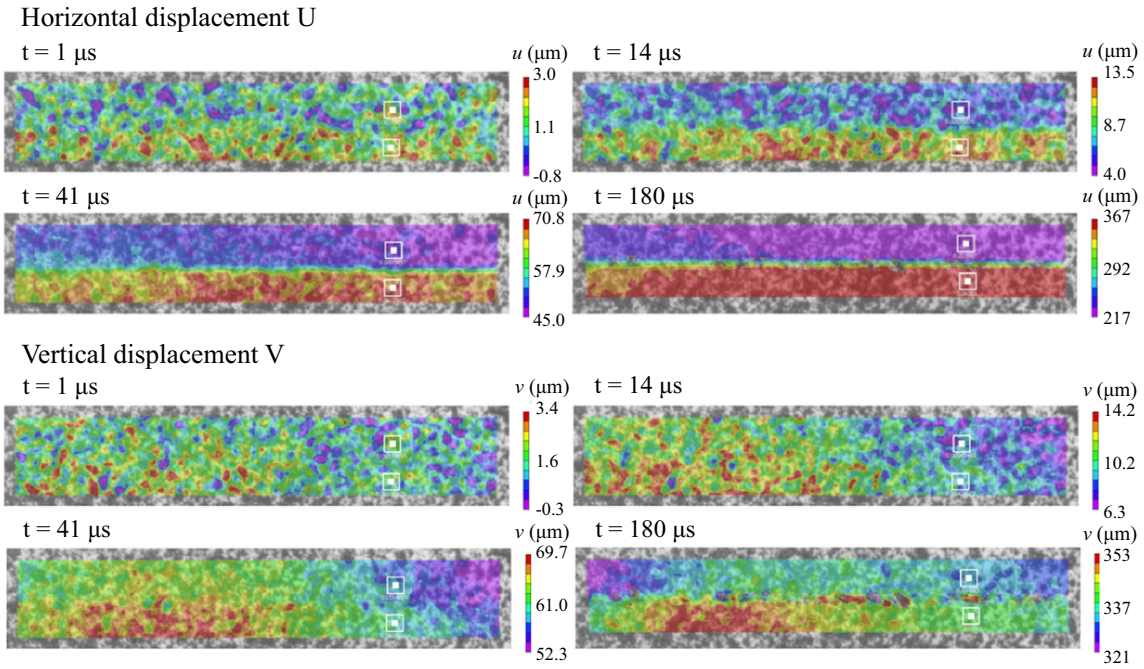

Fig. 16 Horizontal (top) and vertical (bottom) displacement field measured by DIC for the 45° loading condition at $v = 5.8$ m/s at different times: 1 μs, 14 μs, 41 μs and 180 μs

solve 1-μm displacements which set the minimal strain detection to 5.10^{-3}.

Normalized strains at failure are listed for all tests in Table 6. For each loading condition, a good repeatability is observed. In addition, the 45° and 75° loading conditions present similar shear strains at failure. The discrepancy may be explained by different compressive strains at failure. Indeed, the compressive strain seems to reduce the effectiveness of shear on crack propagation. Much lower shear strains at failure are observed for the 15° loading condition than for the other conditions. This is a consequence of the formation of the tensile stress component in this condition and the subsequent occurence of a mixed shear/traction crack propagation.

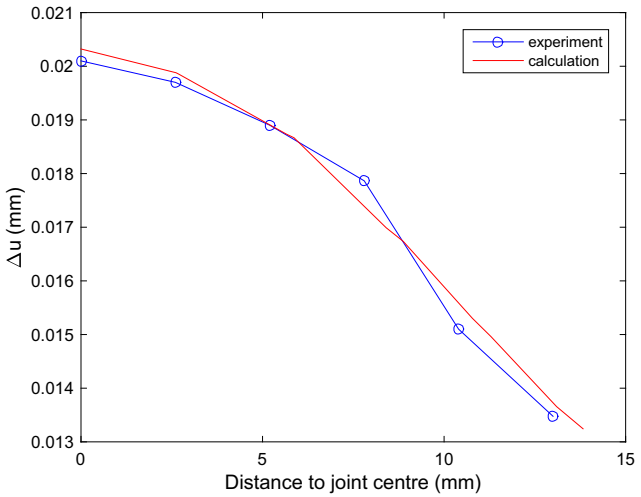

Fig. 17 Experimental and numerical horizontal displacement jump for the 45° loading condition at $v = 5.8$ m/s at 41 μs. The experimental jumps were measured at 2×6 points spaced at 2.6 mm

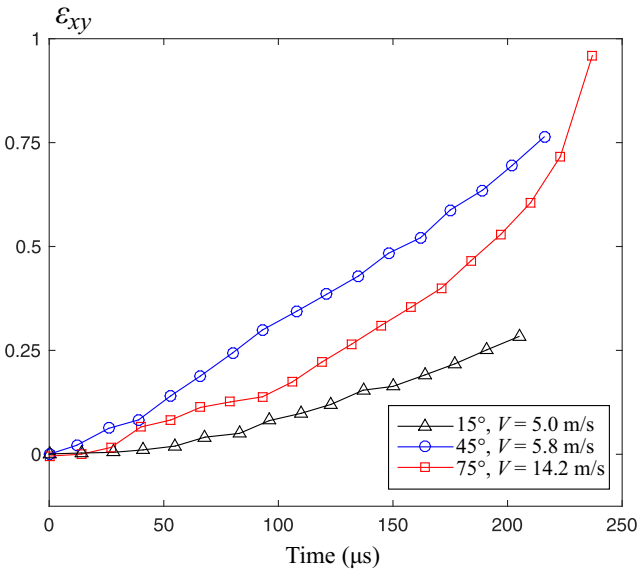

Fig. 18 Normalized shear strain ε_{xy} measured at the joint center as a function of time for the 15°, 45° and 75° loading conditions

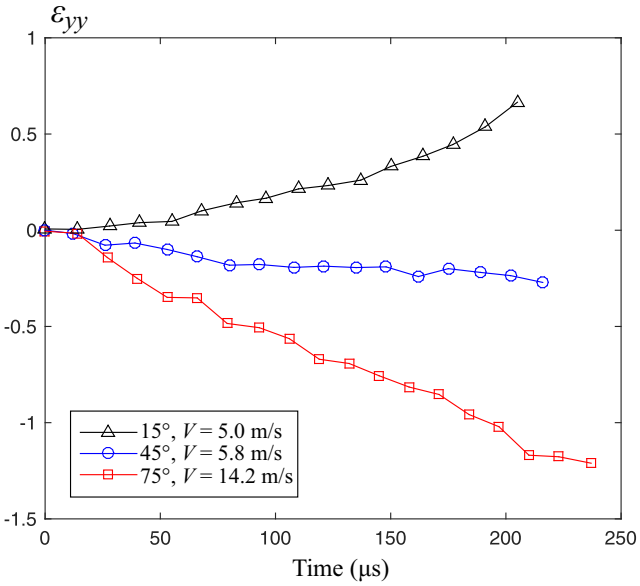

Fig. 19 Normalized normal strain ε_{yy} measured at the joint center as a function of time for the 15°, 45° and 75° loading conditions

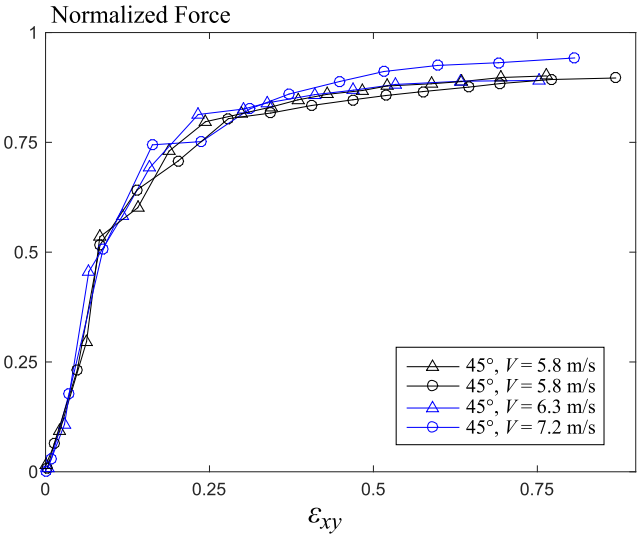

Fig. 20 Normalized global force as a function of normalized shear strain ε_{xy} at the joint center for the 45° loading conditions

Local Stress Measurement and Joint Behavior

Even though the measured force at the specimen/output bar interface provides information about the complete assembly only, one can present the global force against the local shear strain measured with DIC. Thus, an approximate behavior of the joint is obtained and presented in Fig. 20 with a good reproducibility among the different experiments. This analysis supposes that the local shear strain at the joint center represents the shear stress state along the complete joint length which is unrealistic in Fig. 7. Another approach is presented in the next paragraph.

Table 6 Summary of normalized failure strain for all tested specimens

Loading condition	Shear strain at failure	Normal strain at failure
15°	0.27	0.70
15°	0.13	0.25
15°	0.20	0.35
45°	0.80	−0.15
45°	0.75	−0.25
45°	0.78	−0.20
45°	0.87	−0.15
75°	0.98	−1.30
75°	0.91	−1.10
75°	0.95	−1.20

The material behavior of the joint can be derived from the proposed measurements. Local stress estimation in the joint can be performed and inferred directly from the DIC measurement. Thus, the behavior of the adhesive joint can be estimated without the development of a numerical inverse method. Indeed, the displacement fields can be post-treated by Vic2D to compute the strain fields. As already mentioned, this procedure amplifies the measurement noise. However, uncertainties related to the numerical derivation can be reduced by increasing the subset size in the correlation. Thus, strain measurements are obtained in the aluminum adherents near the adhesive joint, for instance, as shown in Fig. 21. The virtual gauge (white rectangle) is set to 100×15 pixels to measure the local stresses in the center. The virtual gauge size has also been increased to reduce measurement noise due to numerical derivation. Several assumptions are needed to infer the stresses from the measured strains. Since surface measurements are collected, a plane stress state is assumed. Dynamic characterization of the aluminum adherent alone enabled us to identify material parameters (i.e., Young's modulus E^*, the shear modulus G^* and Poisson's ratio ν^*). Elastic behavior is assumed in

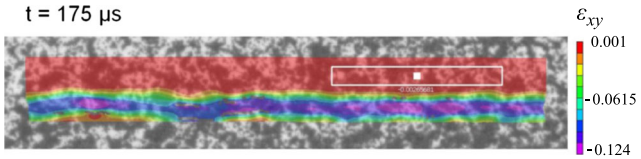

Fig. 21 Shear strain field obtained by DIC for the 45° loading condition at 175 μs

the aluminum. The stresses in the aluminum adherent are given as a function of the strains:

$$\sigma_{yy} = \frac{E^*}{1-(\nu^*)^2}\left(\varepsilon_{yy} + \nu^*\varepsilon_{xx}\right) \text{ and } \sigma_{xy} = 2G^*\varepsilon_{xy} \quad (5)$$

Thus, one can measure stresses in the aluminum close to the adherent/joint boundary and infer stresses in the joint due to the continuity of normal stress (i.e., σ_{yy} and σ_{xy}) through the interface. However, the stress component σ_{yy} is very difficult to measure in the aluminum adherent because ε_{xx} and ε_{yy} are needed and the measurement noise of each signal accumulates. In addition, ε_{yy} is very noisy because there are very few pixels along the y-direction. In this contribution, this stress component is not proposed.

The shear strain ε_{xy} in the adherent is presented in Fig. 21 for the 45° loading condition at 175 μs. In this figure, the red part corresponds to the strain in the adherent, and the highly deformed purple part corresponds to the strain in the joint. However, the strains in the adhesive part cannot be used because there are too few pixels there; therefore, the strains in this part may not be accurate.

The shear stress in the virtual gauge is then obtained from (equation (5)). The stresses in the joint are assumed to be homogeneous along the joint thickness (y-direction). By relating this stress measurement and the strain measurement detailed in Section "Local Measurements", an estimation of the experimental behavior of the joint can be derived. The normalized results are presented in Fig. 22 for the 15° and 45° loading conditions. Results are not presented for the 75° loading condition, as the aluminum reaches the yield limit during the experiment and subsequently exhibits plastic behavior during this test. Elasto-plastic parameters of the joint can be estimated from the Fig. 22. They are shown in Table 7. As expected, both the 15° and 45° loading conditions exhibit the same shear modulus for the adhesive, but with different yield and failure stresses. This is a well-known phenomenon for polymers, as both yield and failure stresses increase with increasing hydrostatic pressure. Finally, the 45°-yield stress is higher than the 15°-yield stress because of the presence of a compressive stress in the test at 45°.

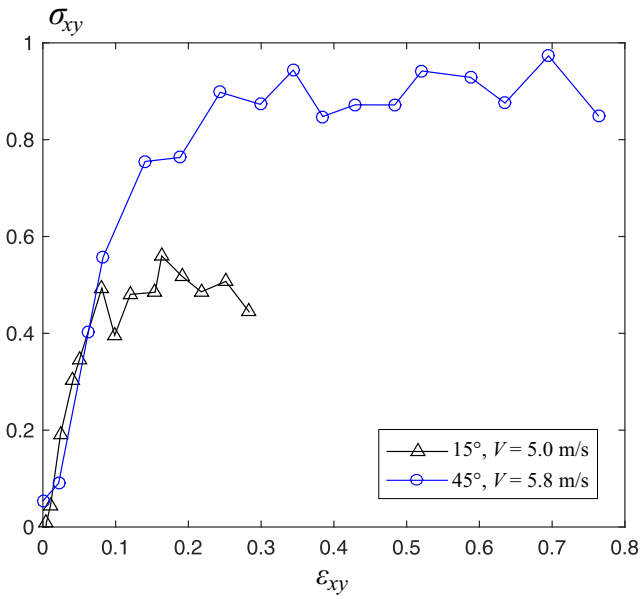

Fig. 22 Adhesive joint behavior identified on 15° and 45° loading conditions: normalized shear stress σ_{xy} as a function of normalized shear strain ε_{xy}

Table 7 Identification of normalized elasto-plastic parameters from Fig. 22

Loading angle	15°	45°
G	5.9	6.2
σ_y	0.4	0.6

Conclusion

This paper presented a novel specimen dedicated for use in dynamic and multiaxial testing of adhesive joints. The general method to characterize the material behavior of an adhesive joint includes combining a classic split Hopkinson pressure bar analysis with local displacement measurements performed by high-speed image acquisition and digital image correlation. The innovative *DODECA* specimen allows three different impact loadings, which represent three different stress states to test. Several simple assumptions on the local displacement field enabled us to estimate the local strain and stress in the adhesive joint and to deduce the material behavior of the joint. In addition, strains at the failure point are also an interesting result of the proposed experimental procedure.

The introduction of DIC to the dynamic characterization of adhesive joints provides a new means for developing new testing experiments for the characterization of adhesive joints. This is particularly interesting because of the non-uniformity of the strain field in a specimen designed for adhesive joints testing. This work will contribute to a better understanding of the material response of adhesive joints.

Further work is still necessary to better interpret the presented measurements. In particular, numerical inverse methods would be useful to identify the complete behavior of the adhesive joint by minimization procedures. The inverse calculation would require an accurate numerical dynamic model able to represent both force and local displacements within a reasonable calculation time.

Acknowledgements Authors thank Philippe Chevallier (LMS) for his help with experiments and Gerard Gary (LMS) for his useful advice on dynamic experiments.

References

1. Cognard JY, Créachcadec R, Sohier L, Davies P (2008) Analysis of the nonlinear behavior of adhesives in bonded assembliesComparison of TAST and Arcan tests. Int J Adhes Adhes 28(8):393–404
2. Carrere N, Badulescu C, Cognard JY, Leguillon D (2015) 3D models of specimens with a scarf joint to test the adhesive and cohesive multi-axial behavior of adhesives. Int J Adhes Adhes 62:154–164
3. Adamvalli M, Parameswaran V (2008) Dynamic strength of adhesive single lap joints at high temperature. Int J Adhes Adhes 28(6):321–327
4. Challita G, Othman R (2010) Finite-element analysis of SHPB tests on double-lap adhesive joints. Int J Adhes Adhes 30(4):236–244
5. Challita G, Othman R, Casari P, Khalil K (2011) Experimental investigation of the shear dynamic behavior of double-lap adhesively bonded joints on a wide range of strain rates. Int J Adhes Adhes 31(3):146–153
6. Halary JL, Lauprêtre F (2015) Mécanique des matériaux polymères. Belin
7. Raykhere SL, Kumar P, Singh R, Parameswaran V (2010) Dynamic shear strength of adhesive joints made of metallic and composite adherents. Mater Des 31(4):2102–2109
8. Roth CC, Gary G, Mohr D (2015) Compact SHPB system for intermediate and high strain rate plasticity and fracture testing of sheet metal. Exper Mech 55:1803–1811
9. Rittel D, Maigre H (1996) An investigation of dynamic crack initiation in PMMA. Mech Mater 23(3):229–239
10. Zhao J, Knauss W, Ravichandran G (2009) A new shear-compression-specimen for determining quasistatic and dynamic polymer properties. Exper Mech 49(3):427
11. Dorogoy A, Rittel D, Godinger A (2016) A shear-tension specimen for large strain testing. Exp Mech 56(3):437–449
12. Kuhn P, Catalanotti G, Xavier J, Camanho PP, Koerber H (2017) Fracture toughness and crack resistance curves for fiber compressive failure mode in polymer composites under high rate loading. Compos Struct 182:164–175
13. Zhou J, Wang Y, Xia Y (2006) Mode-I fracture toughness of PMMA at high loading rates. J Mater Sci 41(24):8363–8366
14. Wang Q, Feng F, Ni M, Gou X (2011) Measurement of mode I and mode II rock dynamic fracture toughness with cracked straight through flattened Brazilian disc impacted by split Hopkinson pressure bar. Eng Fract Mech 78(12):2455–2469
15. Banks-Sills L, Schwartz J (2002) Fracture testing of Brazilian disk sandwich specimens. Int J Fract 118(3):191–209
16. Martin E, Pavia F, Ventrella A, Avalle M, Lara-Curzio E, Ferraris M (2012) A Brazilian disk test for the evaluation of the shear strength of epoxy-joined ceramics. Int J Appl Ceram Technol 9(4):808–815
17. Janin A, Constantinescu A, Weisz-Patrault D, Neviere R, Stackler M, Albouy W (2017) An experimental technique for the characterization of adhesive joints under dynamic multiaxial loadings. Procedia Eng 197:52–59
18. Thevamaran R, Daraio C (2014) An experimental technique for the dynamic characterization of soft complex materials. Exp Mech 54(8):1319–1328
19. Zhang Q, Zhao J (2014) Quasi-static and dynamic fracture behaviour of rock materials: phenomena and mechanisms. Int J Fract 189(1):1–32
20. Hild F, Roux S (2006) Digital image correlation: from displacement measurement to identification of elastic properties–a review. Strain 42(2):69–80
21. Roux S, Hild F (2006) Stress intensity factor measurements from digital image correlation: post-processing and integrated approaches. Int J Fract 140(1):141–157
22. Gilat A, Schmidt T, Walker A (2009) Full field strain measurement in compression and tensile split Hopkinson bar experiments. Exp Mech 49(2):291–302
23. Koerber H, Xavier J, Camanho P (2010) High strain rate characterisation of unidirectional carbon-epoxy IM7-8552 in transverse compression and in-plane shear using digital image correlation. Mech Mater 42(11):1004–1019
24. Seidt J, Kuokkala V, Smith J, Gilat A (2016) Synchronous full-field strain and temperature measurement in tensile tests at low, intermediate and high strain rates. Exp Mech 2(57):219–229
25. Reu P (2014) All about speckles: aliasing. Exp Tech 38(5):1–3
26. Kolsky H (1949) An investigation of the mechanical properties of materials at very high rates of loading. Proc Phys Soc Sec B 62(11):676
27. Gary G (2001) Comportement des métaux à grande vitesse de déformation. Modélisation. Ed. Techniques Ingénieur
28. Jiang F, Vecchio KS (2009) Hopkinson bar loaded fracture experimental technique: a critical review of dynamic fracture toughness tests. Appl Mech Rev 62(6):060,802
29. Chen WW, Song B (2010) Split Hopkinson (Kolsky) bar: design, testing and applications. Springer Science & Business Media
30. Gary G (2005) DAVID instruction manual. LMS, Palaiseau
31. Safa K, Gary G (2010) Displacement correction for punching at a dynamically loaded bar end. Int J Impact Eng 37(4):371–384
32. Manual, Abaqus Users (2010) Version 6.10. ABAQUS Inc
33. Cognard JY, Créachcadec R, Sohier L, Leguillon D (2010) Influence of adhesive thickness on the behaviour of bonded assemblies under shear loadings using a modified TAST fixture. Int J Adhes Adhes 30(5):257–266
34. Leguillon D, Sanchez-Palencia E (1987) Computation of singular solutions in elliptic problems and elasticity. Wiley